iScience

CellPress
OPEN ACCESS

Review

Ultraflexible Neural Electrodes for Long-Lasting Intracortical Recording

Fei He,[1,2] Roy Lycke,[1,2,3] Mehran Ganji,[1,2,3] Chong Xie,[1,2,4] and Lan Luan[1,2,4,5,*]

SUMMARY

Implanted electrodes provide one of the most important neurotechniques for fundamental and translational neurosciences by permitting time-resolved electrical detection of individual neurons *in vivo*. However, conventional rigid electrodes typically cannot provide stable, long-lasting recordings. Numerous interwoven biotic and abiotic factors at the tissue-electrode interface lead to short- and long-term instability of the recording performance. Making neural electrodes flexible provides a promising approach to mitigate these challenges on the implants and at the tissue-electrode interface. Here we review the recent progress of ultraflexible neural electrodes and discuss the engineering principles, the material properties, and the implantation strategies to achieve stable tissue-electrode interface and reliable unit recordings in living brains.

INTRODUCTION

Neural circuits process information through temporal sequences of short electrical pulses in neurons. Intracortical recording, the electrophysiologic technique that involves inserting an electrode or electrode array into living brain tissue, can conveniently record these electrical activities. The neural signals recorded extracellularly by penetrating electrodes can be processed to extract information in different frequency bands. The lower-frequency signals, local field potentials (LFPs), reflect collective transmembrane currents from a small volume of the nervous tissue, and the action potentials at higher frequency bands, on the timescale of milliseconds ("spikes"), are generated by the impulses from individual neurons (Figure 1). LFPs, which represent the synchronized input locally, have a critical role in coordinating the activity of neuronal assemblies distributed in the brain for complex processes and functions. Typically they reflect the sum of action potentials from cells within approximately 50–350 μm from the tip of the electrode (Gray et al., 1995; Legatt et al., 1980) and slower ionic events from within 0.5–3 mm from the tip of the electrode (Juergens et al., 1999), but the exact detection range depends on the neuroanatomy as well as the electrode dimension and impedance. In contrast, recordings of extracellular action potentials, or single-unit spikes, require close proximity of the recording electrodes and the cell. Intuitively, inserting microelectrodes into brain tissues achieves this spatial proximity because neurons are packed at a high density in the brain. However, maintaining the spatial proximity and stability over time becomes challenging, which results in instability and degradation of recordings. In this review, we focus on the challenges to improve the stability and longevity of recording extracellular action potentials from the perspective of electrode's form factors and material properties. We outline the considerations of flexible materials and the engineering principles to construct flexible and ultraflexible neural electrodes and discuss how these physical properties improve both the biotic and abiotic stability in intracortical recordings. The article does not have extensive discussions of animal models or biological details in cellular responses to implants, which was nicely summarized in previous review articles (Feiner and Dvir, 2017; Salatino et al., 2017).

CHALLENGES FOR LONG-LASTING NEURAL RECORDINGS

Conventional rigid electrodes such as micro-wires, tetrodes, and micro-fabricated silicon microelectrodes have contributed tremendously to fundamental and translational neurosciences (Alivisatos et al., 2012; Birmingham et al., 2014; Collinger et al., 2013; Nicolelis, 2001; Perlmutter and Mink, 2006; Shen, 2013; Spira and Hai, 2013). However, they often fail to provide reliable recordings that track the same individual neurons over even short periods (hours to days) (Gilletti and Muthuswamy, 2006; Perge et al., 2013), and their performance typically deteriorates over longer periods (weeks, months, and years) (Fraser and Schwartz, 2012; Prasad et al., 2012, 2014; Williams et al., 1999). This is mainly due to the relatively large dimensions of these implants and the consequential surgical injuries, their material and structural instability in the

[1]Department of Electrical and Computer Engineering, Rice University, 6100 Main Street, Houston, TX 77005, USA

[2]NeuroEngineering Initiative, Rice University, 6500 Main Street, Houston, TX 77005, USA

[3]Department of Biomedical Engineering, University of Texas at Austin, 107 Dean Keeton, Austin, TX 78712, USA

[4]Department of Bioengineering, Rice University, 6100 Main Street, Houston, TX 77005, USA

[5]Lead Contact

*Correspondence: lan.luan@rice.edu

https://doi.org/10.1016/j.isci.2020.101387

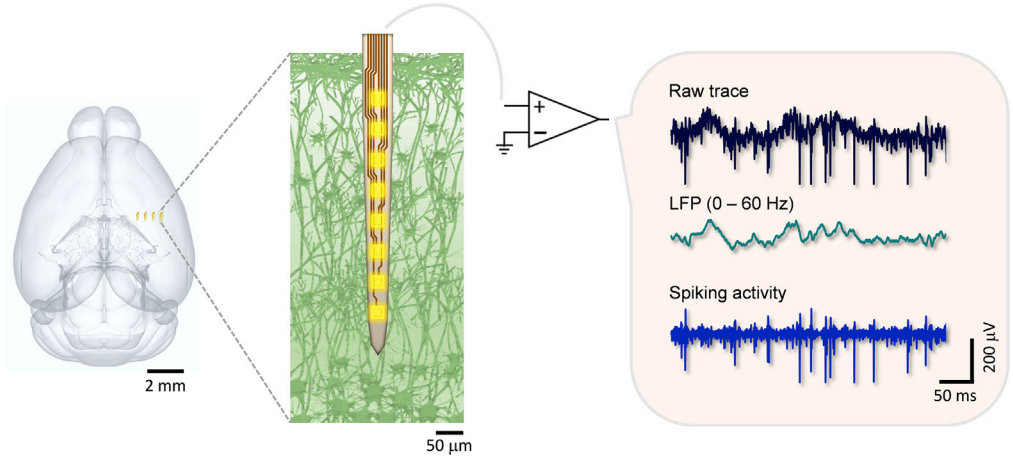

Figure 1. Schematics Showing the Basic Principles of Extracellular Electrophysiological Recording in the Brain

A 4-shank neural probe is implanted in the mouse brain; a zoom-in view of the microlectrodes in neural tissue (left). The raw traces of bioelectrical signals (top right) they record are band-pass filtered at low frequencies to provide local field potentials (middle right) that are the collective electrical potentials from a small volume of the neural tissue. The high-pass-filtered signals are the spiking activities (bottom right) from a single neuron (single-unit action potential) or a few neurons (multi-units). The brain sketch in the left panel is rendered from the Allen Mouse Brain Atlas (Bakker et al., 2015; Lein et al., 2007).

post-implantation conditions, and their relatively strong chronic invasiveness to the surrounding tissue (Grill et al., 2009; Polikov et al., 2005; Rousche and Normann, 1998). In the short term, the mechanical mismatch between tissue and implants induces reoccurring electrode movements from target neurons in response to natural body motions (Gilletti and Muthuswamy, 2006). This leads to sudden waveform changes in time scales as short as hours and prevents reliable tracking of individual neurons over days and longer (Fraser and Schwartz, 2012; Perge et al., 2013). In the long term, the presence of implants causes reoccurring cellular and vascular damage and elicits sustained inflammation and tissue response (Williams et al., 1999) that results in neuronal degeneration and glial scar formation near the implants (Jeong et al., 2015; Seymour and Kipke, 2007; Zhong and Bellamkonda, 2008). Moreover, the stress induced on the implants by the micromotions of surrounding tissues also leads to mechanical damage of the neural electrodes, resulting in premature device failures (Gilgunn et al., 2013; Kozai et al., 2015a; Prasad et al., 2012, 2014). All these chronic deteriorations are manifested in electrical recordings as loss in recording fidelity and efficacy (Gray et al., 1995; Jeong et al., 2015; Kipke et al., 2003; Nicolelis et al., 2003; Rousche and Normann, 1998).

Among the extensive efforts targeting these multifaceted challenges that impeded long-lasting, stable neural recording, growing emphasis was devoted on reducing the neuro-inflammatory response (Feiner and Dvir, 2017; Salatino et al., 2017). Consequently, there is increasing awareness that reducing the neural electrode's dimension (Seymour and Kipke, 2006) and rigidity (Jeong et al., 2015; Kim et al., 2013b; Sohal et al., 2014) could suppress the neuro-inflammatory response and improve the tissue-electrode interface (Jeong et al., 2015). The concept of reducing the mechanical mismatch between implants and tissue to improve tissue-electrode interface have fueled the development of flexible neural electrodes in the past decade. Flexible, biocompatible polymers, such as parylene C (Castagnola et al., 2015; Kim et al., 2013a; Noh et al., 2004; Weltman et al., 2016; Xu et al., 2018), polyimide (Jeon et al., 2014; Mercanzini et al., 2008; Rousche et al., 2001), and SU-8 (Robin et al., 2014; Xu et al., 2016), with a Young's modulus of only a few GPa, were used as the substrates for neural electrodes. Alternatively, a mechanically compliant layer was coated on stiff electrodes; unconventional shapes and geometries were employed to reduce mechanical stiffness (Sohal et al., 2014). Multifunctional flexible probes were also developed using polymer substrates, such as flexible electrodes co-fabricated with micro-light-emitting diodes for simultaneous optogenetic stimulation (Kim et al., 2013b), and microelectrodes in combination with microchannels for local drug delivery (John et al., 2011). However, there were still notable tissue responses to these flexible implants. Consistently, long-lasting recordings of individual neurons were still difficult. It is worth noting that these flexible electrodes, while being more mechanically compliant than rigid electrodes, are still orders of magnitude stiffer than the brain tissue.

Considering these previous efforts in improving the neural-electrode interface, we summarize the following key aspects for establishing reliable and glial-scar-free neural-probe interface: (1) the electrode has sufficient flexibility to ensure complete compliance to tissue micro-movements and to substantially reduce the tissue-electrode interfacial force, (2) the electrode is mechanically and electrically robust for long-term functioning in physiological conditions, (3) the dimension of the electrode is comparable to or smaller than that of average cells and capillaries so that its perturbation to the host biological matrix is minimal (Seymour and Kipke, 2006, 2007), and (4) surgical damage is controlled and minimized during implantation to allow for tissue recovery (Kozai et al., 2014; Potter et al., 2012). In addition to these challenges, it further necessitates a strategy to identify and track the action potentials fired by the same neurons over an extended period of time. Finally, because basic and clinical applications of neural recording often benefit from including a large number of neurons, scalable neural electrodes are highly desired. We discuss below the design rationales of tissue-compliant electrodes and implantation strategies to meet these stringent requirements.

ELECTRODE FORM FACTOR AND MECHANICAL COMPLIANCE

Micromotions around the implanted electrode are thought to play an important role in chronic inflammation and astroglial scarring (Turner et al., 1999). The finite element method analysis on a single silicon microelectrode showed that the longitudinal loading force when deflecting the electrode was a key factor determining the micromotion-induced strain of tissue and the subsequent tissue response (Lee et al., 2005). We, therefore, consider the bending stiffness K, the ratio between the longitudinal loading force and the displacement, as the mechanical characteristics of the tissue-electrode interface. For a single shank that has the geometry of a slab, K can be estimated as (Steif, 2012)

$$K = E_s \frac{wh^3}{12}, \qquad \text{(Equation 1)}$$

where E_s is Young's modulus of the material and h and w are the total thickness and width of the slab, respectively. The bending stiffness K scales with material rigidity (Young's modulus) linearly but scales with the shank thickness to the third power. For a cylindrical beam, K can be estimated as (Steif, 2012)

$$K = E_s \pi \frac{d^4}{64}, \qquad \text{(Equation 2)}$$

where E_s is Young's modulus of the material and d is the diameter of the beam. The Euler buckling force F_B is geometry dependent, and it is given by:

$$F_B = \frac{\pi^2 EI}{(k_e L)^2}, \qquad \text{(Equation 3)}$$

where $E$is the Young's modulus of shuttle device material, $I = (\pi/2)r^4$is the moment of inertia of the cylindrical micro-wire (r is the micro-wire radius) and $I = wh(w^2+h^2)/12$ for the slab geometry, L is the effective length of the cylinder, and $k_e$is the column effective length factor that depends on the boundary conditions and is of the order of 1. Table 1 compares the mechanical characteristics of typical neural electrodes, computed assuming a hypothetical implanted length of 1 mm. We include both the shank (slab) and cylindrical probe geometries and consider rigid and soft materials that have been used to construct neural electrodes such as silicon, parylene, polyimide, polydimethylsiloxane (PDMS), and SU-8. Although reducing the material's Young's modulus reduces the bending stiffness linearly, no material can construct electrodes with sufficient structural and electrical integrity in long-term physiological conditions while approaching the brain's softness. Very soft materials such as hydrogel are too electrically leaky to serve as reliable insulation for neural electrodes. Alternatively, the mechanical compliance of the device depends strongly on its geometry, which permits the drastic reduction of the bending stiffness of electrodes by engineering their form factors.

Figure 2 shows the bending stiffness K and the averaged footprint of electrodes (cross-sectional area divided by the typical number of recording sites in a 1-mm implantation section). Compared with conventional neural electrodes (Kim et al., 2013b; Kozai et al., 2012a; Lee et al., 2005), the recent ultraflexible electrodes at a total thickness of about 1 μm, such as the mesh electrodes (Xie et al., 2015), the nanoelectronic threads (NETs) (Luan et al., 2017; Wei et al., 2018), and the later varieties of similar designs (Ferro et al., 2018; Guan et al., 2019; Yang et al., 2019), have drastically reduced the effective bending stiffness and the average footprint per recording site. Specifically, the bending stiffness is reduced by orders of

Material	Young's Modulus (GPa)	Shape	Dimension ($w \times h$ for Slab)	Bending Stiffness (pNm^2)	Critical Buckling Load (mN)
Silicon (Du et al., 2017; Subbaroyan et al., 2005)	179	Slab L = 1 mm	50 μm × 15 μm	2.52×10^3	300.8
Parylene-C (Castagnola et al., 2015; Kim et al., 2013a; Noh et al., 2004; Weltman et al., 2016; Xu et al., 2018)	3	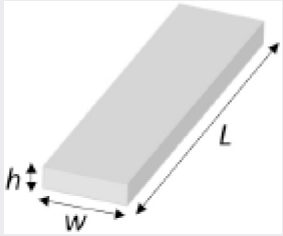	50 μm × 15 μm	42.2	5.04
Polyimide (Jeon et al., 2014; Mercanzini et al., 2008; Rousche et al., 2001)	2.5		50 μm × 15 μm	35.2	4.20
SU-8 (Robin et al., 2014; Xu et al., 2016)	2.3		50 μm × 15 μm	32.3	3.87
SU-8 (Luan et al., 2017; Xie et al., 2015)	2.3		50 μm × 1 μm	0.0096	0.2366
SU-8 (Luan et al., 2017; Wei et al., 2018)	2.3		10 μm × 1 μm	.0019	1.9×10^{-3}
SU-8 (Yang et al., 2019)	2.3		4 μm × 1 μm	7.7×10^{-4}	1.29×10^{-4}
Carbon nanotube multilayer (Zhang et al., 2013)	202		50 μm × 15 μm	2.84×10^3	339.5
PDMS (Minev et al., 2012)	3.6×10^{-3}		50 μm × 15 μm	0.05	6.1×10^{-3}
Nanocomposite (poly(vinylacetate) and cellulose) (Harris et al., 2011)	0.012		50 μm × 15 μm	0.17	0.0202
Soft OSTE (thiol-ene-epoxy) (Lee et al., 2017)	6×10^{-3}		50 μm × 15 μm	0.084	0.0101
Soft elastomeric conducting wire (Du et al., 2017)	9.74×10^{-4}		50 μm × 15 μm	0.014	1.6×10^{-3}
Stainless steel (Thelin et al., 2011)	200	Wire L = 1 mm	d = 50 μm	6.14×10^4	1,211
Tungsten (Harris et al., 2011)	411	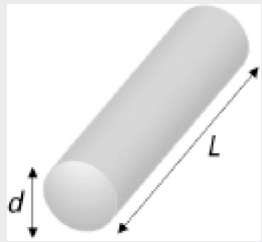	d = 50 μm	1.26×10^5	2,489
Carbon fiber (Kozai et al., 2012a)	234		d = 7.5 μm	36.3	0.717
Carbon nanotube (Xie et al., 2012)	950		d = 150 nm L = 1.5 μm	2.36×10^{-5}	0.207

Table 1. Mechanical Characteristics of Neural Electrodes

magnitude to 10^{-15} N·m^2, which brings down the probe-tissue interfacial force to nanonewton range, on par with the single-cell traction force (du Roure et al., 2005). This is conceived to be the key parameter for improved biocompatibility.

Ultrathin Profile Mitigates the Challenges in Structural and Electrical Stability

The long-term structural integrity of neural electrodes in physiological conditions has been a great challenge. Strong, inert materials are typically used to construct rigid electrodes, but structural failures often

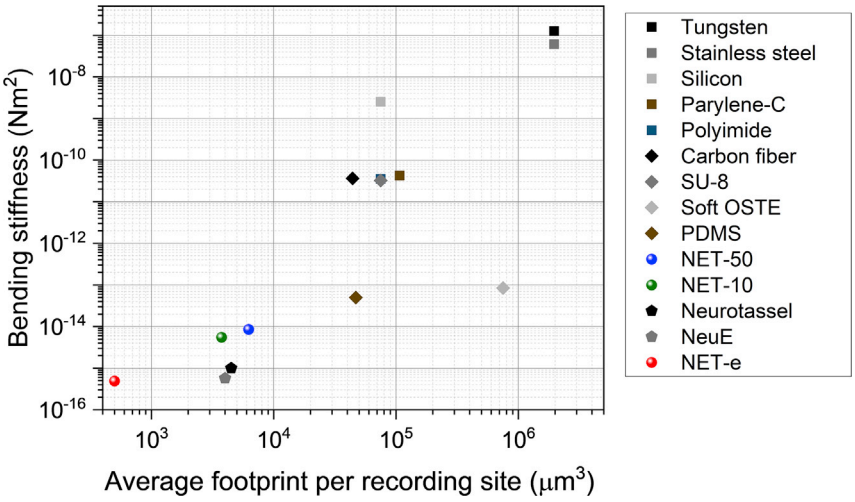

Figure 2. Comparison of the Two Key Aspects of Neural Electrodes Contributing to the Potential Tissue Invasiveness, Averaged Footprint Per Recording Site, and Bending Stiffness (*K*)

Recording contact per 1 mm length is 10 for silicon (Lee et al., 2005), polyimide (Rousche et al., 2001), and SU-8 (Robin et al., 2014; Xu et al., 2016) electrodes; 16 for PDMS (Minev et al., 2012) electrodes; 8 for NET-50 (Luan et al., 2017) and NET-e (Wei et al., 2018); 7 for parylene C electrodes (Kim et al., 2013a); 4 for NET-10 (Luan et al., 2017); and 1 for NeuE (Yang et al., 2019), Neurotassel (Guan et al., 2019), carbon fiber (Kozai et al., 2012a), soft OSTE (Lee et al., 2017), tungsten (Du et al., 2017), and stainless-steel (Thelin et al., 2011) probes. The smallest cross-sectional dimensions are chosen if the references report multiple designs.

arise after long-term implantation in living brains. Structural failures such as cracking and delamination of the insulating materials are manifested in recordings as increased leakage and cross talk. Mechanical strains built up in the device during micromotion are thought to be a major contributor to initiate and accelerate most failure modes (Gilgunn et al., 2013; Kozai et al., 2015a; Prasad et al., 2012, 2014). For instance, delamination between two bonded materials such as the insulating layer and the substrate is typically caused by the built-up strain and the weak bonding between the two different materials (Gilgunn et al., 2013; Kozai et al., 2015a; Prasad et al., 2012, 2014).

One approach to enhance the structural stability, which might be counterintuitive, is to reduce the strain by reducing the device thickness. Using a simplified slab model, the strain in the slab is proportional to its overall thickness at the same deformation (Figure 3A). Therefore, by reducing the thickness of the slab we reduce the built-up strain linearly. Neural electrodes typically have more complicated mechanics because they are constructed by multiple materials for different functions, such as metals for electrical connectivity and inert materials for structural support and electrical insulation. A symmetric profile, e.g., all metal interconnect leads are buried in the center of the device by the same material at an equal thickness (Figure 3B), will help to further mitigate strain-related issues.

The approach of reducing thickness has been successfully implemented to construct flexible neural electrodes to promote structural integrity (Hong and Lieber, 2019; Jeong et al., 2015; Rivnay et al., 2017). As one example, we outline the structure of the ultraflexible NET. A multilayer, symmetric architecture was employed to construct NETs. Metal trace lines were embedded between two layers of 500-nm-thick SU-8 thin films. Recording contacts were patterned on the top and bottom surfaces, which made electrical connections with the trace lines through "vertical interconnect access (via)" (Figure 3B). After microfabrication, the devices were hard-baked to promote SU-8–SU-8 fusion. The 1-μm-thick NET was able to bend at a curvature of about 50 μm while maintaining its structural and electrical integrity (Figure 3C), which strongly supports the design rationale that ultrathin structures have enhanced resistance to defects induced by deformation. Similarly, other ultraflexible electrodes at about the same thickness (Guan et al., 2019; Xie et al., 2015) exhibit a similar level of mechanical compliance and structural durability upon deformation (Figures 3D and 3E).

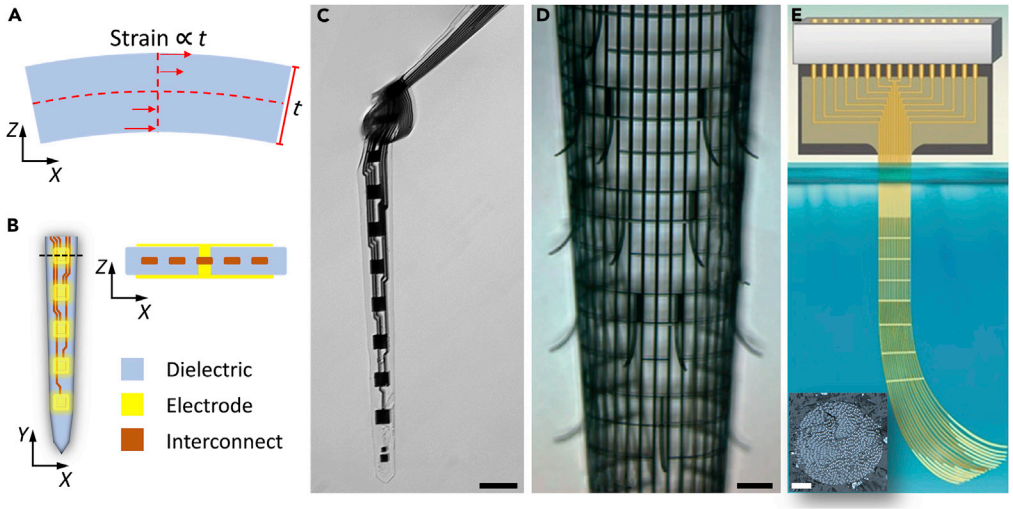

Figure 3. Ultrathin Profile Enhances the Structural Integrity of Neural Electrodes by Reducing the Strain

(A) Sketch showing that under the same deformation, strain in a device is proportional to its thickness.

(B) Sketch showing a symmetric, multilayer profile to minimize strain.

(C–E) Examples of ultraflexible electrodes, including a NET-50 suspended in water (C, *Figure reprinted from Sci. Adv. 3 e1601966* (Luan et al., 2017) *with permission. Copyright 2017 AAAS*), a macroporous mesh suspended in buffer (D, *Figure reprinted from Nature Materials 14, 1286 (2015)* (Xie et al., 2015) *with permission. Copyright 2015 NPG publishing*), and a Neurotassel in the molten PEG (E, *Figure reprinted from Science advances 5.3 (2019): eaav2842* (Guan et al., 2019) *with permission. Copyright 2019 AAAS publishing*). Scale bars: 50 μm in (C), 100 μm in (D), and 20 μm in (inset in E).

In addition to strain-related issues, insufficient binding between the different materials often causes delamination failures (Gilgunn et al., 2013; Kozai et al., 2015a; Prasad et al., 2012, 2014). Depending on the materials multiple approaches are effective in improving the bonding strength. Take the two materials SU-8 and polyimide for flexible neural electrodes as examples: multiple layers of photoresist SU-8 can be thermally cross linked at hard-baking temperature 190–195°C to promote diffusion at the interface and to form a monolithic piece (Luan et al., 2017; Xie et al., 2015; Zhao et al., 2017). Adhesion-promoting layers such as SiC and diamond-like carbon are deposited on metal trace lines to improve the adhesion with polyimide (Ordonez et al., 2012; Tooker et al., 2012).

Another typical delamination failure happens between micro-lithographically defined contact sites and their functional coatings. For example, conducting polymers (CPs), have emerged as promising interfacing material between biomedical devices and neural tissue due to their superior electrochemical and compliant (soft) mechanical properties for conforming to biological tissue compared with conventional metals such as Au, Pt, and Ir (Ganji et al., 2018; Khodagholy et al., 2015). However, exploiting the full capability of CP coatings in chronic biomedical applications has been limited due to their weak adhesion and mechanical stability by lack of strong covalent bonds between coated polymer layers and underlying noble metal conductors (Gerwig et al., 2012; Im et al., 2007). Two approaches were introduced to tackle this problem. The first approach utilizes an intermediate functionalized monolayer to form stable covalent bonds between the CP and the underlying metal interconnect (Wei et al., 2015). The second approach employs more engaged surface area and mechanical interlocking to anchor the coated CP to underlying metals including "Fuzzy gold" stabilization for polypyrrole (PPy) (Cui and Martin, 2003), IrOx and nanostructured Pt for PEDOT (Boehler et al., 2017), laser-roughened Pt anchoring for PEDOT/p-toluenesulfonate (Green et al., 2012), and gold nanorods (Au-nr) for stabilizing PEDOT:PSS polymer film (Ganji et al., 2018).

One important challenge for polymer-based flexible devices is that almost all polymers absorb water (Tan and Craighead, 2010), which may further cause leakage by themselves (Lu et al., 1998), and more importantly, expedite the aforementioned mechanical degradations. Polymers at low water absorption rates such as polyimide (0.7 wt %) are generally preferred material choices to construct neural electrodes. For any given polymer, increasing polymer thickness improves the water resistance, but it compromises the flexibility of the electrode and may lead to mechanical failures due to increased strain as discussed earlier. Another approach without changing the electrode form factors is to reduce the metal trace linewidth and

consequently reduce the capacitive coupling of the metal trace lines to the electrolyte in the tissue. We note that mild water absorption itself in polymer does not severely compromise the recording efficacy. Taking SU-8 as an example, water absorption in SU-8 saturates at about 3.3 wt % (Tam and Lau, 2015), but the SU-8-constructed NETs recorded extracellular action potentials exceeding 800 μV in amplitudes during long-term implantation without a longitudinal decay in signal-to-noise ratio (Luan et al., 2017). This suggests that in the absence of other mechanical failures such as cracking and delamination, water absorption in the polymer itself may not strongly affect the dielectric properties of the material.

STRATEGIES TO IMPLANT ULTRAFLEXIBLE ELECTRODES WITH MINIMAL SURGICAL FOOTPRINTS

There is an intrinsic conflict on the requirement of an electrode's rigidity between minimal invasiveness and facile insertion into the brain with minimal damage. The miniature dimension and ultraflexibility desired for minimizing tissue response mechanically preclude the electrode's self-supported penetration through brain tissue. One common strategy to deliver flexible electrodes is to temporarily alter the electrode's rigidity before and during insertion (Hassler et al., 2011; Khaled et al., 2013; Patel et al., 2015; Takeuchi et al., 2004; Wu et al., 2015). Biodegradable materials, such as polyethylene glycol (PEG) (Patel et al., 2015; Takeuchi et al., 2004), silk (Wu et al., 2015), and carboxymethyl cellulose (Kozai et al., 2014), have been used to temporarily encapsulate and rigidify neural electrodes to support the penetration into the brain tissue. Shortly after implantation, the coated material is dissolved and the neural electrode is exposed. Alternatively, unconventional electrode substrate materials that reduce stiffness after implantation were used, such as the mechanically adaptive nanocomposite (Harris et al., 2011) or shape memory polymer (Ware et al., 2014). Temporarily freezing the electrode in a small amount of solution was also demonstrated for stereotaxic insertion (Xie et al., 2015). One caveat of this approach is that the supporting materials all have relatively small Young's moduli (<10 GPa), and therefore thick coatings (>50 μm) and large cross section are required to achieve enough rigidity for insertion, which induces significant implantation injury irrespective of the dimension for the electrodes. To mitigate this problem, a microfluidic device was developed to deliver flexible electrodes deep into neural tissue without increasing the stiffness or size of the electrodes. The microfluidic device applies a tension force to ultraflexible electrodes that prevents buckling and permits precisely actuating the electrode position with micron-scale accuracy (Vitale et al., 2018).

The other approach is to use a separate rigid shuttle device that is later decoupled from the electrode (Felix et al., 2013; Kim et al., 2013b; Kozai and Kipke, 2009; Liu et al., 2015; Sohal et al., 2014). Syringe injection was developed to drive ultraflexible mesh electrodes in solution through a needle. The flexible mesh subsequently relaxes and interpenetrates within the internal space of the brain (Liu et al., 2015). Alternatively, stiffeners fabricated of silicon or metal wires are temporarily attached to the flexible electrodes by biodegradable adhesive such as PEG (Felix et al., 2013; Joo et al., 2019; Kim et al., 2013b; Kozai and Kipke, 2009; Zhao et al., 2019) or by geometrical anchors (Kim et al., 2013a). The electrode and stiffener are surgically implanted together; then the temporary attachment disengages to allow for retraction of the stiffener without moving the implanted electrode out of the tissue. Although this approach involves additional fabrication and assembling of shuttle devices and can potentially add a level of complexity to the flexible electrode packing, it permits using a wide variety of materials and reducing the total surgical footprints.

To minimize the acute tissue damage, a shuttle device with the smallest dimension is desired. The lower limit of the shuttle device cross section is set by the mechanical strength needed to break through the brain tissue during insertion without bulking or breaking, which requires the buckling force to be larger than the insertion force. Therefore, materials with the largest elastic moduli are desired to reduce the surgical footprint and the consequential tissue damage.

Table 2 summarizes the diameter of a microbeam that permits 1 mN bulking force, which is comparable to the insertion force of a much larger neural electrode reported in the literature (Sharp et al., 2009), and the minimum diameter that supports self-penetration estimated from a recent work that accounted for the geometrical scaling effect (Obaid et al., 2018). Straightforwardly, materials with large elastic moduli such as diamonds, carbon fiber, and tungsten permit penetrating the brain tissue at reduced beam diameters. Among them, silicon can be readily microfabricated, and both carbon fiber and tungsten micro-wires are commercially available at low costs, making them affordable candidates to construct shuttle devices at minimal footprints.

Materials	Diamond (Klein and Cardinale, 1993)	Carbon fiber (Kozai et al., 2012a)	Tungsten (Du et al., 2017)	Silicon (Joo et al., 2019)	SU-8 (Lorenz et al., 1997)	Polyimide (Rousche et al., 2001)	PEG (Paxton et al., 2009)
Young's modulus (GPa)	1,100	234	411	179	2.3	2.5	1.3
d at 1 mN bulking force (μm)	7.4	10.9	10.0	11.5	34.4	33.8	39.8
Min *d* (μm)	3.1	5.1	4.3	5.6	22.8	22.2	27.5

Table 2. Beam Diameter to Permit Pia Penetration

Figure 4 demonstrates the shuttle-assisted implantation of various flexible electrodes using both the strategy of geometrical anchor (Figures 4A and 4B) and temporary adhesion (Figures 4C and 4D). Figure 4A shows an example of a temporary geometrical attaching mechanism. A micro-pole, 2 μm in diameter and 5 μm in height, micro-milled at the end of the shuttle device is temporarily engaged through a micro-hole at the end of an ultra-flexible neural electrode (Luan et al., 2017). During implantation the shuttle device travels into the tissue; the anchor post enters into the hole and pulls the neural electrode into the brain tissue. Once the neural electrode reaches the desired depth, the shuttle device is retracted vertically and the neural electrode is released and left embedded in the brain tissue. This needle-and-thread mechanism was first demonstrated as a manual procedure. Later, the same principle was applied to design and construct a "sewing machine" that enabled delivering hundreds and thousands of flexible electrodes at a high throughput (Musk, 2019) (Figure 4B). Alternatively, shuttle devices were fabricated and assembled before surgery (Figures 4C and 4D) using biodissolvable adhesive. Figure 4C shows an example of aligning tungsten micro-wires (diameters ranging 20–50 μm) into pre-patterned grooves or fixation and then attaching them to multi-shank flexible electrodes using water-soluble PEG (Zhao et al., 2019). After the assembled electrode-shuttle pairs were inserted into the targeted brain region, the PEG was dissolved and then the shuttle device was retracted.

It is worth noting that substantial difficulty of insertion comes from penetrating connective tissue—the dura, arachnoid, and pia mater—that together protect the brain from mechanical and other insults (Weller et al., 2018). A durotomy is often performed before implantation to reduce the insertion force, but this additional invasive procedure adds surgical complications and sometimes affects the recording performance. One way to enable insertion without increasing the diameter of shuttle devices is to reduce the effective force on the device by fabricating a sharper tip (Figure 4D) (Bjornsson et al., 2006; Jensen et al., 2006; Sharp et al., 2009). A recent development on 3D-sharpened silicon shuttle has validated the dural-penetrating shuttle in combination with a flexible polymer probe for chronic recordings. The sharpened shuttle limited brain compression and obviates a durotomy in rats and reduced post-surgical edema, which would also likely increase accuracy in depth targeting of the electrode arrays (Joo et al., 2019).

ULTRAFLEXIBLE ELECTRODES REDUCE TISSUE RESPONSE AND PERMIT GLIA-SCAR-FREE INTERFACE

Brain tissue response to neural electrode involves entangled reactions by multiple types of surrounding cells (e.g., neurons, astrocytes, microglia, and more) and interactions with the neurovascular system (Grill et al., 2009; Kozai et al., 2015b; McConnell et al., 2009; Polikov et al., 2005). These dynamic events cover time scales ranging from minutes to weeks (Johnson et al., 2006; Kozai et al., 2012b). The most common method to evaluate the tissue response is to perform postmortem histology studies that provide "snapshot" images of specific cells and biomarkers at the tissue-electrode interface. Time-dependent histology was used to study how the implanted ultraflexible electrodes affected the distribution of key cell types such as neurons and astrocytes across the hippocampus and cortex in transgenic mice as a function of time post-implantation (Yang et al., 2019). Reconstructed histological images in 3D showed a relatively uniform cell distribution without obvious depletion of neurons or enhancements of astrocytes near the ultraflexible electrodes from the earliest time of analysis (Figure 5A). These observations were consistent with earlier (Hong et al., 2018; Luan et al., 2017; Wei et al., 2018; Xie et al., 2015) and later works (Guan et al., 2019) of flexible electrodes with similar form factors and supported the validity of using ultraflexible polymer-based devices for a stable tissue-electrode interface.

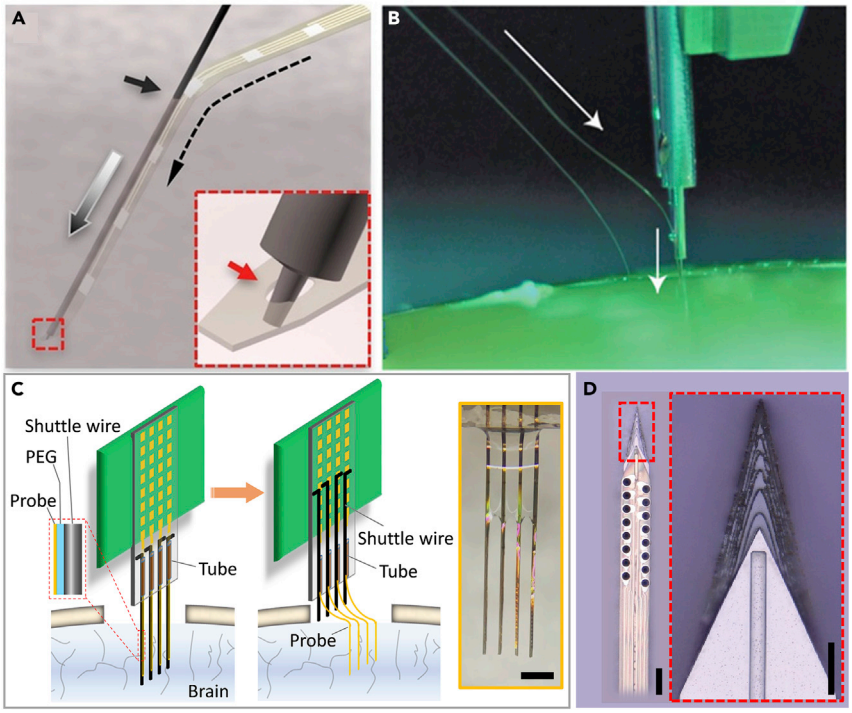

Figure 4. Shuttle-Assisted Implantation of Ultraflexible Neural Electrodes

(A) Schematic showing the needle-thread temporary engaging mechanism. Inset: Zoom-in sketch highlighting that the micro-post engages in the micro-hole on a NET. *Figure adapted from Sci. Adv. 3 e1601966* (Luan et al., 2017) *with permission. Copyright 2017 AAAS.*

(B) Photograph of the insertion process with a "sewing machine." Arrows indicate a needle penetrating tissue proxy, advancing the thread to the desired depth. *Figure reprinted from J Med Internet Res 2019; 21(10):e16194* (Musk, 2019) *with permission. Copyright 2019 Journal of Medical Internet Research.*

(C) Sketch demonstrating the temporary adhesion between shuttle wires and the neural electrodes. Inset shows a photograph of the NET-shuttle pairs before implantation.

(D) Optical micrograph of a polymer neural probe mounted on a sharpened silicon shuttle. Inset: Zoom-in view of the top of a sharpened silicon shuttle and wicking channel for PEG at midline. *Figure reprinted from Journal of Neural Engineering 16.6 (2019): 066021* (Joo et al., 2019) *with permission. Copyright 2019 IOP.* Scale bars: 500 μm in (inset in C), 100 μm in (D), and 50 μm in (inset in D).

In addition, *in vivo* imaging in the brain combined with fluorescent labeling techniques has emerged as a powerful tool to dissect the underlying mechanism of tissue reactions to neural electrodes (Kozai et al., 2010, 2012b). Recently, important advances have been made on direct imaging of the electrode-tissue interface, which has revealed dynamic information of acute tissue reactions (Eles et al., 2019; Kozai et al., 2015b; Wellman et al., 2019). More importantly, longitudinal *in vivo* imaging permits repeated mapping and tracking of the tissue-electrode interface and unambiguously reveals the dynamic process of tissue responses over a long period. For example, 3D stacks of two-photon (2P) imaging were collected for up to 3.5 months post-surgery to track the changes in capillaries, astrocytes, and neurons around the NETs (Luan et al., 2017). The time sequence of vasculature over 2 months showed that the surgical damage leads to minor local leakage of brain-blood barrier (BBB) upon implantation, which lasted for at most 1 month and was fully repaired in association with vascular remodeling. By two months NETs were embedded in capillaries with normal density, intact BBB, and normal microcirculation (Figure 5B). All neurons in the vicinity of NETs were repeatedly identified in later imaging sessions, which suggested that NETs induced no chronic neuronal loss. The astrocytes near the NET surrounded only capillaries with normal density and morphology without accumulation or encapsulation at the NET (Figures 5C and 5D). These imaging results were consistent with postmortem histology studies. They provided valuable insight into the time-dependent evolution of the tissue-electrode interface and the stability of neural recordings.

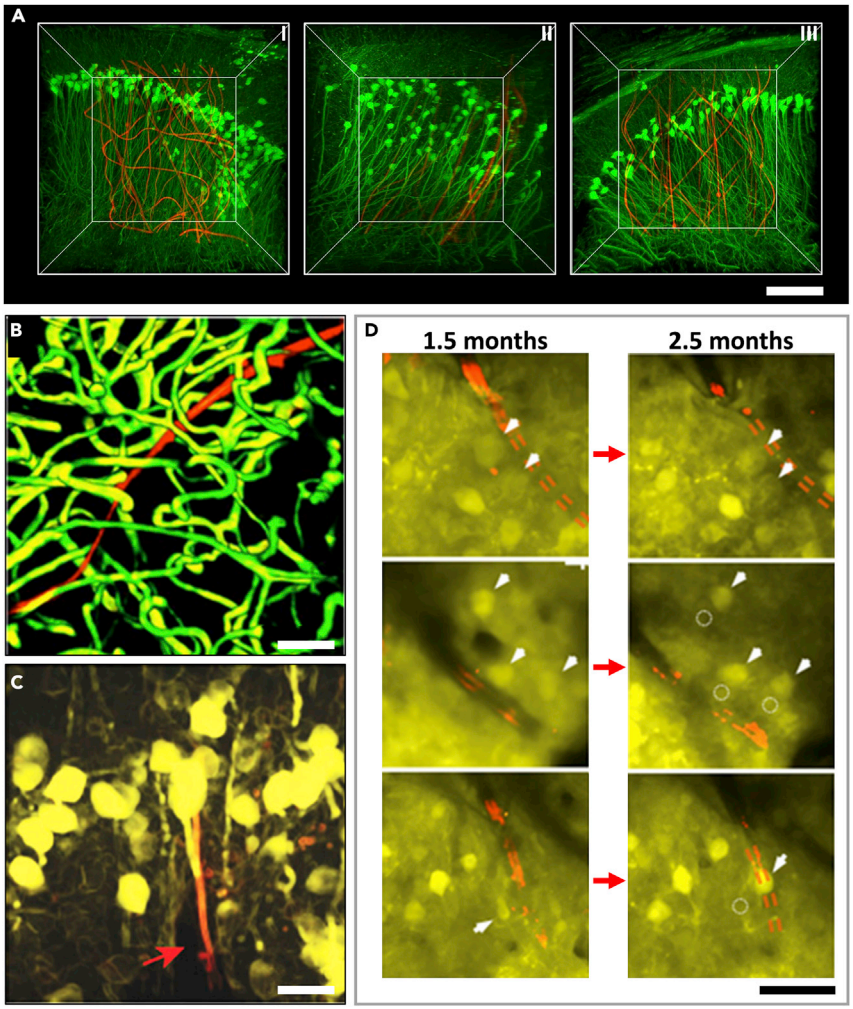

Figure 5. Imaging and Tracking of the Cellular and Vascular Networks at the Chronic Interfaces between Ultraflexible Electrodes and Neural Tissues

(A) Time-dependent 3D histology of interfaces between NeuE (red) and neurons (green) showing a relatively uniform cell distribution at 2 days (I), 2 weeks (II), and 3 months (III) post-implantation. *Figure reprinted from Nature Materials 18, 510* (Yang et al., 2019) *with permission. Copyright 2019 NPG publishing.*

(B) 3D reconstruction of vasculatures by *in vivo* 2P microscopy around a NET-10 probe (red) 2 months after implantation, highlighting fully recovered capillary networks (green). Image stack: 100–320 μm below a mouse brain surface. *Figure reprinted from Sci. Adv. 3 e1601966* (Luan et al., 2017) *with permission. Copyright 2017 AAAS.*

(C) 3D reconstruction of *in vivo* 2P images of neurons (yellow) in Thy1-YFP mice surrounding a NET-e probe (red) 2 months after implantation. The NET-e is denoted by a red arrow. Image stack: 100–320 μm below the brain surface. *Figure reprinted from Advanced Science 5.6 (2018): 1700625* (Wei et al., 2018) *with permission. Copyright 2018 Wiley.*

(D) Representative *in vivo* 2P images from the same regions showing that neurons are repeatedly identified at different times after implantation. Red: NET-10. Arrows and dashed circles highlight the current and previous locations of neurons, respectively. *Figure adapted from Sci. Adv. 3 e1601966* (Luan et al., 2017) *with permission. Copyright 2017 AAAS.* Scale bars: 100 μm in (A), 50 μm in (B and D), and 10 μm in (C).

EMERGING OPPORTUNITIES

Ultraflexible neural electrodes have demonstrated their unique strengths in several applications. First, they are well suited to be combined with longitudinal *in vivo* optical imaging. These ultraflexible electrodes such as NETs bend without breaking, and radii of curvature of <100 μm are achievable. This means that one or more devices can be inserted underneath or through small holes in an imaging window and then bent out of the way. This flexibility facilitates optical access and circumvents the geometrical constrains of placing

rigid electrodes at oblique penetrations to avoid interference with the microscope objective (Poskanzer and Yuste, 2016). The compatibility with optical imaging was used to directly visualize and track the probe-tissue interface longitudinally (Luan et al., 2017; Wei et al., 2018). The optical modality can also be used to map other brain activities such as cerebral blood flow (Dunn et al., 2001; Kazmi et al., 2013) and blood oxygenation (Sullender et al., 2018) to permit simultaneous measurements of multiple neurophysiological parameters (Luan et al., 2018). Furthermore, these ultraflexible electrodes induce minimal or little perturbation to the baseline physiology and allow for long-lasting, stable neural recordings. Therefore, they are well suited to track brain dysfunctions over chronic time scales that are commensurate with the progression and recovery of brain injuries. A recent study using ultraflexible NETs and laser speckle contrast imaging revealed long-lasting, injury-dependent neurovascular dissociations after small-scale strokes in rodent models. Neuronal deficits extend spatiotemporally, whereas restoration of cerebral blood flow occurs sooner and reaches a higher relative value, which informs the limitation of neuroimaging techniques that infer neural activity from hemodynamic responses (He et al., 2020). Last, the uncoventional form factors of these electrodes enable unconventional implantation and recordings to regions that are difficult to reach otherwise. A recent study reports chronically stable *in vivo* recordings from retinal ganglion cells in awake mice using epiretinal-implanted ultraflexible mesh electronics delivered via noncoaxial and minimally invasive intravitreal injection to form a chronically stable conformal retina interface. Such a method provides an attractive alternative to past studies in explants and offers important new insights into the dynamic information processing between the retina and other parts of the nervous system (Hong et al., 2018).

FUTURE CHALLENGES

Although flexible neural electrodes have demonstrated great advantages over rigid devices in terms of biocompatibility, recording longevity, and compatibility with optical imaging techniques, their flexibility makes surgical implantation more challenging. Although multiple strategies have been developed and successfully tested in rodents, the surgery or the pre-surgery packaging of flexible devices remains more demanding than the rigid electrodes. Furthermore, many of the implantation strategies do not permit simultaneous recording during insertion or fine control of the insertion speed, which is necessary for targeting specific brain regions such as the hippocampus. For instance, if the flexible probe is bonded to the shuttle device temporarily using a biodegradable adhesive, the insertion speed is limited by the dissolution time of the adhesive, which may lead to premature separation of the electrode from the shuttles when targeting deep brain regions. In addition, the adhesive may also cover the recording contacts, making it impossible to record neural activity during insertion. Further refinement of implantation techniques such as testing biodegradable materials that have longer and controllable dissolution times, such as silk (Wu et al., 2011), and refining a strategy using geometrical anchors (Luan et al., 2017) would enable recording during insertion. Machining jigs and fixtures for shuttle devices will simplify the procedure and minimize human errors.

Most of the ultraflexible electrodes have only been tested in a few brain areas, with the greatest success in the superficial cortex. Additional refined designs are needed to optimize recording for different brain regions, where cell density varies substantially and current experiments cannot customize state-of-the-art devices to maximize yield across regions. For example, whereas cells are broadly spatially distributed in the neocortex, in the hippocampus the excitatory cells are localized to thin, densely packed layers. Electrode design parameters such as contact size, contact spacing, and spatial distribution need to be tested, refined, and optimized for the anatomic structures, depths, and neuronal densities of multiple brain regions and species.

OUTLOOK AND PROSPECTS

With nearly 100 billion neurons and 100 trillion connections, understanding the brain remains one of the greatest challenges in both science and engineering. To better understand how brains function and dysfunction, we need to develop technologies that can decipher this massively interconnected network. These technologies need to cover diverse time scales, ranging from moment-by-moment information processing occurring at milliseconds to neural plasticity that spans a lifetime and underlies development, learning, and aging. These technologies also need to have broad spatial coverage because neural circuits consist not only of nearby populations of neurons but also of neurons distributed across multiple areas in the brain. Finally, these technologies need to provide high spatial specificity to accurately investigate the many cell types in the brain as neural circuits are composed of varied neurons with unique physiological and structural characteristics. Ultraflexible neural electrodes provide great promise to address these unmet

needs. We envision that future technology development will enable (1) long-term recording of extracellular action potentials that lasts years or even decades; (2) large-scale, high-channel-count recordings that are distributed across the brain (Chung et al., 2019) or closely packed at high volumetric density; and (3) convenient integration with other techniques such as optical imaging and spike sorting to provide cell-type information. Combining all these aspects, ultraflexible neural electrodes will continue to enable discoveries in fundamental and translational neuroscience.

ACKNOWLEDGMENTS

This work was supported by National Institute of Neurological Disorders and Stroke through R01NS109361(L.L.) and R01NS102917(C.X.), by National Heart, Lung, and Blood Institute under K25HL140153 (L.L.), and by the Welch foundation Research grant #F-1941-20170325 (C.X.).

AUTHOR CONTRIBUTIONS

L.L. outlined the manuscript. F.H., R.L., and M.G. prepared figures and tables. All authors wrote the manuscript. L.L. led the work.

DECLARATION OF INTERESTS

C.X. and L.L. are co-inventors on a patent on the ultraflexible neural electrode technology filed by the University of Texas. L.L. and C.X. hold equity ownership in Neuralthread Inc., an entity that is licensing this technology. All other authors declare no competing interests.

REFERENCES

Alivisatos, A.P., Chun, M., Church, G.M., Greenspan, R.J., Roukes, M.L., and Yuste, R. (2012). The brain activity map project and the challenge of functional connectomics. Neuron *74*, 970–974.

Bakker, R., Tiesinga, P., and Kotter, R. (2015). The scalable brain atlas: instant web-based access to public brain atlases and related content. Neuroinformatics *13*, 353–366.

Birmingham, K., Gradinaru, V., Anikeeva, P., Grill, W.M., Pikov, V., McLaughlin, B., Pasricha, P., Weber, D., Ludwig, K., and Famm, K. (2014). Bioelectronic medicines: a research roadmap. Nat. Rev. Drug Discov. *13*, 399–400.

Bjornsson, C.S., Oh, S.J., Al-Kofahi, Y.A., Lim, Y.J., Smith, K.L., Turner, J.N., De, S., Roysam, B., Shain, W., and Kim, S.J. (2006). Effects of insertion conditions on tissue strain and vascular damage during neuroprosthetic device insertion. J. Neural Eng. *3*, 196–207.

Boehler, C., Oberueber, F., Schlabach, S., Stieglitz, T., and Asplund, M. (2017). Long-term stable Adhesion for conducting polymers in biomedical applications: IrOx and nanostructured platinum solve the chronic challenge. ACS Appl. Mater. Interfaces *9*, 189–197.

Castagnola, V., Descamps, E., Lecestre, A., Dahan, L., Remaud, J., Nowak, L.G., and Bergaud, C. (2015). Parylene-based flexible neural probes with PEDOT coated surface for brain stimulation and recording. Biosens. Bioelectron. *67*, 450–457.

Chung, J.E., Joo, H.R., Fan, J.L., Liu, D.F., Barnett, A.H., Chen, S., Geaghan-Breiner, C., Karlsson, M.P., Karlsson, M., Lee, K.Y., et al. (2019). High-density, long-lasting, and multi-region electrophysiological recordings using polymer electrode arrays. Neuron *101*, 21–31 e25.

Collinger, J.L., Foldes, S., Bruns, T.M., Wodlinger, B., Gaunt, R., and Weber, D.J. (2013). Neuroprosthetic technology for individuals with spinal cord injury. J. Spinal Cord Med. *36*, 258–272.

Cui, X., and Martin, D.C. (2003). Fuzzy gold electrodes for lowering impedance and improving adhesion with electrodeposited conducting polymer films. Sens. Actuators. A Phys. *103*, 384–394.

du Roure, O., Saez, A., Buguin, A., Austin, R.H., Chavrier, P., Silberzan, P., and Ladoux, B. (2005). Force mapping in epithelial cell migration. Proc. Natl. Acad. Sci. U S A *102*, 2390–2395.

Du, Z.J., Kolarcik, C.L., Kozai, T.D.Y., Luebben, S.D., Sapp, S.A., Zheng, X.S., Nabity, J.A., and Cui, X.T. (2017). Ultrasoft microwire neural electrodes improve chronic tissue integration. Acta Biomater. *53*, 46–58.

Dunn, A.K., Bolay, H., Moskowitz, M.A., and Boas, D.A. (2001). Dynamic imaging of cerebral blood flow using laser speckle. J. Cereb. Blood Flow Metab. *21*, 195–201.

Eles, J.R., Vazquez, A.L., Kozai, T.D.Y., and Cui, X.T. (2019). Meningeal inflammatory response and fibrous tissue remodeling around intracortical implants: an in vivo two-photon imaging study. Biomaterials *195*, 111–123.

Feiner, R., and Dvir, T. (2017). Tissue–electronics interfaces: from implantable devices to engineered tissues. Nat. Rev. Mater. *3*, 17076.

Felix, S.H., Shah, K.G., Tolosa, V.M., Sheth, H.J., Tooker, A.C., Delima, T.L., Jadhav, S.P., Frank, L.M., and Pannu, S.S. (2013). Insertion of flexible neural probes using rigid stiffeners attached with biodissolvable adhesive. J. Vis. Exp. *79*, e50609.

Ferro, M.D., Proctor, C.M., Gonzalez, A., Zhao, E., Slezia, A., Pas, J., Dijk, G., Donahue, M.J., Williamson, A., Malliaras, G.G., et al. (2018). NeuroRoots, a bio-inspired, seamless Brain Machine Interface device for long-term recording. bioRxiv, 460949.

Fraser, G.W., and Schwartz, A.B. (2012). Recording from the same neurons chronically in motor cortex. J. Neurophysiol. *107*, 1970–1978.

Ganji, M., Hossain, L., Tanaka, A., Thunemann, M., Halgren, E., Gilja, V., Devor, A., and Dayeh, S.A. (2018). Monolithic and scalable Au nanorod substrates improve PEDOT-metal adhesion and stability in neural electrodes. Adv. Healthc. Mater. *7*, e1800923.

Gerwig, R., Fuchsberger, K., Schroeppel, B., Link, G.S., Heusel, G., Kraushaar, U., Schuhmann, W., Stett, A., and Stelzle, M. (2012). PEDOT-CNT composite microelectrodes for recording and electrostimulation applications: fabrication, morphology, and electrical properties. Front. Neuroeng. *5*, 8.

Gilgunn, P.J., Ong, X.C., Flesher, S.N., Schwartz, A.B., and Gaunt, R.A. (2013). Structural analysis of explanted microelectrode arrays. Int. IEEE EMBS Conf. Neural Eng. 719–722.

Gilletti, A., and Muthuswamy, J. (2006). Brain micromotion around implants in the rodent somatosensory cortex. J. Neural Eng. *3*, 189–195.

Gray, C.M., Maldonado, P.E., Wilson, M., and McNaughton, B. (1995). Tetrodes markedly improve the reliability and yield of multiple single-unit isolation from multi-unit recordings in cat striate cortex. J. Neurosci. Methods *63*, 43–54.

Green, R.A., Hassarati, R.T., Bouchinet, L., Lee, C.S., Cheong, G.L., Yu, J.F., Dodds, C.W., Suaning, G.J., Poole-Warren, L.A., and Lovell, N.H. (2012). Substrate dependent stability of conducting polymer coatings on medical electrodes. Biomaterials *33*, 5875–5886.

Grill, W.M., Norman, S.E., and Bellamkonda, R.V. (2009). Implanted neural interfaces: biochallenges and engineered solutions. Annu. Rev. Biomed. Eng. *11*, 1–24.

Guan, S., Wang, J., Gu, X., Zhao, Y., Hou, R., Fan, H., Zou, L., Gao, L., Du, M., Li, C., et al. (2019). Elastocapillary self-assembled neurotassels for stable neural activity recordings. Sci. Adv. *5*, eaav2842.

Harris, J.P., Capadona, J.R., Miller, R.H., Healy, B.C., Shanmuganathan, K., Rowan, S.J., Weder, C., and Tyler, D.J. (2011). Mechanically adaptive intracortical implants improve the proximity of neuronal cell bodies. J. Neural Eng. *8*, 066011.

Hassler, C., Boretius, T., and Stieglitz, T. (2011). Polymers for neural implants. J. Polym. Sci. Pol. Phys. *49*, 18–33.

He, F., Sullender, C.T., Zhu, H., Williamson, M.R., Li, X., Zhao, Z., Jones, T.A., Xie, C., Dunn, A.K., and Luan, L. (2020). Multimodal mapping of neural activity and cerebral blood flow reveals long-lasting neurovascular dissociations after small-scale strokes. Sci. Adv. *6*, eaba1933.

Hong, G., Fu, T.M., Qiao, M., Viveros, R.D., Yang, X., Zhou, T., Lee, J.M., Park, H.G., Sanes, J.R., and Lieber, C.M. (2018). A method for single-neuron chronic recording from the retina in awake mice. Science *360*, 1447–1451.

Hong, G., and Lieber, C.M. (2019). Novel electrode technologies for neural recordings. Nat. Rev. Neurosci. *20*, 330–345.

Im, S.G., Yoo, P.J., Hammond, P.T., and Gleason, K.K. (2007). Grafted conducting polymer films for nano-patterning onto various organic and inorganic substrates by oxidative chemical vapor deposition. Adv. Mater. *19*, 2863–2867.

Jensen, W., Yoshida, K., and Hofmann, U.G. (2006). In-vivo implant mechanics of flexible, silicon-based ACREO microelectrode arrays in rat cerebral cortex. IEEE Trans. Biomed. Eng. *53*, 934–940.

Jeon, M., Cho, J., Kim, Y.K., Jung, D., Yoon, E.S., Shin, S., and Cho, I.J. (2014). Partially flexible MEMS neural probe composed of polyimide and sucrose gel for reducing brain damage during and after implantation. J. Micromech. Microeng. *24*, 025010.

Jeong, J.W., Shin, G., Park, S.I., Yu, K.J., Xu, L., and Rogers, J.A. (2015). Soft materials in neuroengineering for hard problems in neuroscience. Neuron *86*, 175–186.

John, J., Li, Y., Zhang, J., Loeb, J.A., and Xu, Y. (2011). Microfabrication of 3D neural probes with combined electrical and chemical interfaces. J. Micromech. Microeng. *21*, 105011.

Johnson, M.D., Langhals, N.B., and Kipke, D.R. (2006). Neural interface dynamics following insertion of hydrous iridium oxide microelectrode arrays. Conf. Proc. IEEE Eng. Med. Biol. Soc. *1*, 3178–3181.

Joo, H.R., Fan, J.L., Chen, S., Pebbles, J.A., Liang, H., Chung, J.E., Yorita, A.M., Tooker, A.C., Tolosa, V.M., Geaghan-Breiner, C., et al. (2019). A microfabricated, 3D-sharpened silicon shuttle for insertion of flexible electrode arrays through dura mater into brain. J. Neural Eng. *16*, 066021.

Juergens, E., Guettler, A., and Eckhorn, R. (1999). Visual stimulation elicits locked and induced gamma oscillations in monkey intracortical- and EEG-potentials, but not in human EEG. Exp. Brain Res. *129*, 247–259.

Kazmi, S.M., Parthasarthy, A.B., Song, N.E., Jones, T.A., and Dunn, A.K. (2013). Chronic imaging of cortical blood flow using Multi-Exposure Speckle Imaging. J. Cereb. Blood Flow Metab. *33*, 798–808.

Khaled, I., Elmallah, S., Cheng, C., Moussa, W.A., Mushahwar, V.K., and Elias, A.L. (2013). A flexible base electrode array for intraspinal microstimulation. IEEE Trans. Biomed. Eng. *60*, 2904–2913.

Khodagholy, D., Gelinas, J.N., Thesen, T., Doyle, W., Devinsky, O., Malliaras, G.G., and Buzsaki, G. (2015). NeuroGrid: recording action potentials from the surface of the brain. Nat. Neurosci. *18*, 310–315.

Kim, B.J., Kuo, J.T., Hara, S.A., Lee, C.D., Yu, L., Gutierrez, C.A., Hoang, T.Q., Pikov, V., and Meng, E. (2013a). 3D Parylene sheath neural probe for chronic recordings. J. Neural Eng. *10*, 045002.

Kim, T.I., McCall, J.G., Jung, Y.H., Huang, X., Siuda, E.R., Li, Y., Song, J., Song, Y.M., Pao, H.A., Kim, R.H., et al. (2013b). Injectable, cellular-scale optoelectronics with applications for wireless optogenetics. Science *340*, 211–216.

Kipke, D.R., Vetter, R.J., Williams, J.C., and Hetke, J.F. (2003). Silicon-substrate intracortical microelectrode arrays for long-term recording of neuronal spike activity in cerebral cortex. IEEE Trans. Neural Syst. Rehabil. Eng. *11*, 151–155.

Klein, C.C., and Cardinale, G.F. (1993). Young's modulus and Poisson's ratio of CVD diamond. Diamond Relat. Mater. *2*, 918–923.

Kozai, T.D., Catt, K., Li, X., Gugel, Z.V., Olafsson, V.T., Vazquez, A.L., and Cui, X.T. (2015a). Mechanical failure modes of chronically implanted planar silicon-based neural probes for laminar recording. Biomaterials *37*, 25–39.

Kozai, T.D., Jaquins-Gerstl, A.S., Vazquez, A.L., Michael, A.C., and Cui, X.T. (2015b). Brain tissue responses to neural implants impact signal sensitivity and intervention strategies. ACS Chem. Neurosci. *6*, 48–67.

Kozai, T.D., and Kipke, D.R. (2009). Insertion shuttle with carboxyl terminated self-assembled monolayer coatings for implanting flexible polymer neural probes in the brain. J. Neurosci. Methods *184*, 199–205.

Kozai, T.D., Langhals, N.B., Patel, P.R., Deng, X., Zhang, H., Smith, K.L., Lahann, J., Kotov, N.A., and Kipke, D.R. (2012a). Ultrasmall implantable composite microelectrodes with bioactive surfaces for chronic neural interfaces. Nat. Mater. *11*, 1065–1073.

Kozai, T.D., Marzullo, T.C., Hooi, F., Langhals, N.B., Majewska, A.K., Brown, E.B., and Kipke, D.R. (2010). Reduction of neurovascular damage resulting from microelectrode insertion into the cerebral cortex using in vivo two-photon mapping. J. Neural Eng. *7*, 046011.

Kozai, T.D., Vazquez, A.L., Weaver, C.L., Kim, S.G., and Cui, X.T. (2012b). In vivo two-photon microscopy reveals immediate microglial reaction to implantation of microelectrode through extension of processes. J. Neural Eng. *9*, 066001.

Kozai, T.D.Y., Gugel, Z., Li, X., Gilgunn, P.J., Khilwani, R., Ozdoganlar, O.B., Fedder, G.K., Weber, D.J., and Cui, X.T. (2014). Chronic tissue response to carboxymethyl cellulose based dissolvable insertion needle for ultra-small neural probes. Biomaterials *35*, 9255–9268.

Lee, H., Bellamkonda, R.V., Sun, W., and Levenston, M.E. (2005). Biomechanical analysis of silicon microelectrode-induced strain in the brain. J. Neural Eng. *2*, 81–89.

Lee, H.C., Ejserholm, F., Gaire, J., Currlin, S., Schouenborg, J., Wallman, L., Bengtsson, M., Park, K., and Otto, K.J. (2017). Histological evaluation of flexible neural implants; flexibility limit for reducing the tissue response? J. Neural Eng. *14*, 036026.

Legatt, A.D., Arezzo, J., and Vaughan, H.G., Jr. (1980). Averaged multiple unit activity as an estimate of phasic changes in local neuronal activity: effects of volume-conducted potentials. J. Neurosci. Methods *2*, 203–217.

Lein, E.S., Hawrylycz, M.J., Ao, N., Ayres, M., Bensinger, A., Bernard, A., Boe, A.F., Boguski, M.S., Brockway, K.S., Byrnes, E.J., et al. (2007). Genome-wide atlas of gene expression in the adult mouse brain. Nature *445*, 168–176.

Liu, J., Fu, T.M., Cheng, Z., Hong, G., Zhou, T., Jin, L., Duvvuri, M., Jiang, Z., Kruskal, P., Xie, C., et al. (2015). Syringe-injectable electronics. Nat. Nanotechnology *10*, 629–636.

Lorenz, H., Despont, M., Fahrni, N., LaBianca, N., Renaud, P., and Vettiger, P. (1997). SU-8: a low-cost negative resist for MEMS. J. Micromech. Microeng. *7*, 121–124.

Lu, X., Xu, G., Hofstra, P.G., and Bajcar, R.C. (1998). Moisture-absorption, dielectric relaxation, and thermal conductivity studies of polymer composites. J. Polym. Sci. Pol. Phys. *36*, 2259–2265.

Luan, L., Sullender, C.T., Li, X., Zhao, Z., Zhu, H., Wei, X., Xie, C., and Dunn, A.K. (2018). Nanoelectronics enabled chronic multimodal neural platform in a mouse ischemic model. J. Neurosci. Methods *295*, 68–76.

Luan, L., Wei, X., Zhao, Z., Siegel, J.J., Potnis, O., Tuppen, C.A., Lin, S., Kazmi, S., Fowler, R.A., Holloway, S., et al. (2017). Ultraflexible nanoelectronic probes form reliable, glial scar-free neural integration. Sci. Adv. *3*, e1601966.

McConnell, G.C., Rees, H.D., Levey, A.I., Gutekunst, C.A., Gross, R.E., and Bellamkonda, R.V. (2009). Implanted neural electrodes cause chronic, local inflammation that is correlated with local neurodegeneration. J. Neural Eng. *6*, 056003.

Mercanzini, A., Cheung, K., Buhl, D.L., Boers, M., Maillard, A., Colin, P., Bensadoun, J.C., Bertsch, A., and Renaud, P. (2008). Demonstration of cortical recording using novel flexible polymer neural probes. Sens. Actuators A Phys. *143*, 90–96.

Minev, I.R., Chew, D.J., Delivopoulos, E., Fawcett, J.W., and Lacour, S.P. (2012). High sensitivity recording of afferent nerve activity using ultra-compliant microchannel electrodes: an acute in vivo validation. J. Neural Eng. *9*, 026005.

Musk, E. (2019). An integrated brain-machine interface platform with thousands of channels. J. Med. Internet. Res. *21*, e16194.

Nicolelis, M.A. (2001). Actions from thoughts. Nature *409*, 403–407.

Nicolelis, M.A., Dimitrov, D., Carmena, J.M., Crist, R., Lehew, G., Kralik, J.D., and Wise, S.P. (2003). Chronic, multisite, multielectrode recordings in macaque monkeys. Proc. Natl. Acad. Sci. U S A *100*, 11041–11046.

Noh, H.S., Moon, K.S., Cannon, A., Hesketh, P.J., and Wong, C.P. (2004). Wafer bonding using microwave heating of parylene intermediate layers. J. Micromech. Microeng. *14*, 625–631.

Obaid, A., Wu, Y.-W., Hanna, M., Nix, W., Ding, J., and Melosh, N. (2018). Ultra-sensitive measurement of brain penetration with microscale probes for brain machine interface considerations. bioRxiv *10*, 454520.

Ordonez, J.S., Boehler, C., Schuettler, M., and Stieglitz, T. (2012). Improved polyimide thin-film electrodes for neural implants. Conf. Proc. IEEE Eng. Med. Biol. Soc. *2012*, 5134–5137.

Patel, P.R., Na, K., Zhang, H., Kozai, T.D., Kotov, N.A., Yoon, E., and Chestek, C.A. (2015). Insertion of linear 8.4 mum diameter 16 channel carbon fiber electrode arrays for single unit recordings. J. Neural Eng. *12*, 046009.

Paxton, J.Z., Donnelly, K., Keatch, R.P., and Baar, K. (2009). Engineering the bone-ligament interface using polyethylene glycol diacrylate incorporated with hydroxyapatite. Tissue Eng. Part A *15*, 1201–1209.

Perge, J.A., Homer, M.L., Malik, W.Q., Cash, S., Eskandar, E., Friehs, G., Donoghue, J.P., and Hochberg, L.R. (2013). Intra-day signal instabilities affect decoding performance in an intracortical neural interface system. J. Neural Eng. *10*, 036004.

Perlmutter, J.S., and Mink, J.W. (2006). Deep brain stimulation. Annu. Rev. Neurosci. *29*, 229–257.

Polikov, V.S., Tresco, P.A., and Reichert, W.M. (2005). Response of brain tissue to chronically implanted neural electrodes. J. Neurosci. Methods *148*, 1–18.

Poskanzer, K.E., and Yuste, R. (2016). Astrocytes regulate cortical state switching in vivo. Proc. Natl. Acad. Sci. U S A *113*, E2675–E2684.

Potter, K.A., Buck, A.C., Self, W.K., and Capadona, J.R. (2012). Stab injury and device implantation within the brain results in inversely multiphasic neuroinflammatory and neurodegenerative responses. J. Neural Eng. *9*, 046020.

Prasad, A., Xue, Q.S., Dieme, R., Sankar, V., Mayrand, R.C., Nishida, T., Streit, W.J., and Sanchez, J.C. (2014). Abiotic-biotic characterization of Pt/Ir microelectrode arrays in chronic implants. Front. Neuroeng. *7*, 2.

Prasad, A., Xue, Q.S., Sankar, V., Nishida, T., Shaw, G., Streit, W.J., and Sanchez, J.C. (2012). Comprehensive characterization and failure modes of tungsten microwire arrays in chronic neural implants. J. Neural Eng. *9*, 056015.

Rivnay, J., Wang, H., Fenno, L., Deisseroth, K., and Malliaras, G.G. (2017). Next-generation probes, particles, and proteins for neural interfacing. Sci. Adv. *3*, e1601649.

Robin, C.J., Vishnoi, A., and Jonnalagadda, K.N. (2014). Mechanical behavior and anisotropy of spin-coated SU-8 thin films for MEMS. J. Microelectromech. Syst. *23*, 168–180.

Rousche, P.J., and Normann, R.A. (1998). Chronic recording capability of the Utah Intracortical Electrode Array in cat sensory cortex. J. Neurosci. Methods *82*, 1–15.

Rousche, P.J., Pellinen, D.S., Pivin, D.P., Jr., Williams, J.C., Vetter, R.J., and Kipke, D.R. (2001). Flexible polyimide-based intracortical electrode arrays with bioactive capability. IEEE Trans. Biomed. Eng. *48*, 361–371.

Salatino, J.W., Ludwig, K.A., Kozai, T.D.Y., and Purcell, E.K. (2017). Glial responses to implanted electrodes in the brain. Nat. Biomed. Eng. *1*, 862–877.

Seymour, J.P., and Kipke, D.R. (2006). Fabrication of polymer neural probes with sub-cellular features for reduced tissue encapsulation. Conf. Proc. IEEE Eng. Med. Biol. Soc. *1*, 4606–4609.

Seymour, J.P., and Kipke, D.R. (2007). Neural probe design for reduced tissue encapsulation in CNS. Biomaterials *28*, 3594–3607.

Sharp, A.A., Ortega, A.M., Restrepo, D., Curran-Everett, D., and Gall, K. (2009). In vivo penetration mechanics and mechanical properties of mouse brain tissue at micrometer scales. IEEE Trans. Biomed. Eng. *56*, 45–53.

Shen, H. (2013). Neurotechnology: BRAIN storm. Nature *503*, 26–28.

Sohal, H.S., Jackson, A., Jackson, R., Clowry, G.J., Vassilevski, K., O'Neill, A., and Baker, S.N. (2014). The sinusoidal probe: a new approach to improve electrode longevity. Front. Neuroeng. *7*, 10.

Spira, M.E., and Hai, A. (2013). Multi-electrode array technologies for neuroscience and cardiology. Nat. Nanotechnol. *8*, 83–94.

Steif, P.S. (2012). Mechanics of Materials (Pearson).

Subbaroyan, J., Martin, D.C., and Kipke, D.R. (2005). A finite-element model of the mechanical effects of implantable microelectrodes in the cerebral cortex. J. Neural Eng. *2*, 103–113.

Sullender, C.T., Mark, A.E., Clark, T.A., Esipova, T.V., Vinogradov, S.A., Jones, T.A., and Dunn, A.K. (2018). Imaging of cortical oxygen tension and blood flow following targeted photothrombotic stroke. Neurophotonics *5*, 035003.

Takeuchi, S., Yoshida, Y., Ziegler, D., Mabuchi, K., and Suzuki, T. (2004). Parylene flexible neural probe with micro fluidic channel. Proc. IEEE Micr. Elect. 208–211.

Tam, L.H., and Lau, D. (2015). Moisture effect on the mechanical and interfacial properties of epoxy-bonded material system: an atomistic and experimental investigation. Polymer *57*, 132–142.

Tan, C.P., and Craighead, H.G. (2010). Surface engineering and patterning using parylene for biological applications. Materials *3*, 1803–1832.

Thelin, J., Jorntell, H., Psouni, E., Garwicz, M., Schouenborg, J., Danielsen, N., and Linsmeier, C.E. (2011). Implant size and fixation mode strongly influence tissue reactions in the CNS. PLoS One *6*, e16267.

Tooker, A., Tolosa, V., Shah, K.G., Sheth, H., Felix, S., Delima, T., and Pannu, S. (2012). Polymer neural interface with dual-sided electrodes for neural stimulation and recording. Conf. Proc. IEEE Eng. Med. Biol. Soc. *2012*, 5999–6002.

Turner, J.N., Shain, W., Szarowski, D.H., Andersen, M., Martins, S., Isaacson, M., and Craighead, H. (1999). Cerebral astrocyte response to micromachined silicon implants. Exp. Neurol. *156*, 33–49.

Vitale, F., Vercosa, D.G., Rodriguez, A.V., Pamulapati, S.S., Seibt, F., Lewis, E., Yan, J.S., Badhiwala, K., Adnan, M., Royer-Carfagni, G., et al. (2018). Fluidic microactuation of flexible electrodes for neural recording. Nano Lett. *18*, 326–335.

Ware, T., Simon, D., Liu, C., Musa, T., Vasudevan, S., Sloan, A., Keefer, E.W., Rennaker, R.L., 2nd, and Voit, W. (2014). Thiol-ene/acrylate substrates for softening intracortical electrodes. J. Biomed. Mater. Res. B Appl. Biomater. *102*, 1–11.

Wei, B., Liu, J., Ouyang, L., Kuo, C.C., and Martin, D.C. (2015). Significant enhancement of PEDOT thin film adhesion to inorganic solid substrates with EDOT-acid. ACS Appl. Mater. Interfaces *7*, 15388–15394.

Wei, X., Luan, L., Zhao, Z., Li, X., Zhu, H., Potnis, O., and Xie, C. (2018). Nanofabricated ultraflexible electrode arrays for high-density intracortical recording. Adv. Sci. (Weinh) *5*, 1700625.

Weller, R.O., Sharp, M.M., Christodoulides, M., Carare, R.O., and Mollgard, K. (2018). The meninges as barriers and facilitators for the movement of fluid, cells and pathogens related to the rodent and human CNS. Acta Neuropathol. *135*, 363–385.

Wellman, S.M., Li, L., Yaxiaer, Y., McNamara, I., and Kozai, T.D.Y. (2019). Revealing spatial and temporal patterns of cell death, glial proliferation, and blood-brain barrier dysfunction around implanted intracortical neural interfaces. Front. Neurosci. *13*, 493.

Weltman, A., Yoo, J., and Meng, E. (2016). Flexible, penetrating brain probes enabled by advances in polymer microfabrication. Micromachines (Basel) *7*, 180.

Williams, J.C., Rennaker, R.L., and Kipke, D.R. (1999). Long-term neural recording characteristics of wire microelectrode arrays implanted in cerebral cortex. Brain Res. Brain Res. Protoc. *4*, 303–313.

Wu, F., Im, M., and Yoon, E. (2011). A flexible fish-bone-shaped neural probe strengthened by

biodegradable silk coating for enhanced biocompatibility. Paper presented at: 2011 16th International Solid-State Sensors, Actuators and Microsystems Conference.

Wu, F., Tien, L.W., Chen, F.J., Berke, J.D., Kaplan, D.L., and Yoon, E. (2015). Silk-backed structural optimization of high-density flexible intracortical neural probes. J. Microelectromech. Syst. *24*, 62–69.

Xie, C., Lin, Z., Hanson, L., Cui, Y., and Cui, B. (2012). Intracellular recording of action potentials by nanopillar electroporation. Nat. Nanotechnol. *7*, 185–190.

Xie, C., Liu, J., Fu, T.M., Dai, X., Zhou, W., and Lieber, C.M. (2015). Three-dimensional macroporous nanoelectronic networks as minimally invasive brain probes. Nat. Mater. *14*, 1286–1292.

Xu, H., Hirschberg, A.W., Scholten, K., Berger, T.W., Song, D., and Meng, E. (2018). Acute in vivo testing of a conformal polymer microelectrode array for multi-region hippocampal recordings. J. Neural Eng. *15*, 016017.

Xu, T.G., Yoo, J.H., Babu, S., Roy, S., Lee, J.B., and Lu, H.B. (2016). Characterization of the mechanical behavior of SU-8 at microscale by viscoelastic analysis. J. Micromech. Microeng. *26*, 105001.

Yang, X., Zhou, T., Zwang, T.J., Hong, G., Zhao, Y., Viveros, R.D., Fu, T.M., Gao, T., and Lieber, C.M. (2019). Bioinspired neuron-like electronics. Nat. Mater. *18*, 510–517.

Zhang, H., Patel, P.R., Xie, Z., Swanson, S.D., Wang, X., and Kotov, N.A. (2013). Tissue-compliant neural implants from microfabricated carbon nanotube multilayer composite. ACS Nano *7*, 7619–7629.

Zhao, Z., Li, X., He, F., Wei, X., Lin, S., and Xie, C. (2019). Parallel, minimally-invasive implantation of ultra-flexible neural electrode arrays. J. Neural Eng. *16*, 035001.

Zhao, Z., Luan, L., Wei, X., Zhu, H., Li, X., Lin, S., Siegel, J.J., Chitwood, R.A., and Xie, C. (2017). Nanoelectronic coating enabled versatile multifunctional neural probes. Nano Lett. *17*, 4588–4595.

Zhong, Y., and Bellamkonda, R.V. (2008). Biomaterials for the central nervous system. J. R. Soc. Interface *5*, 957–975.